Horizontal Divergence and Vertical Velocity Retrievals from Doppler Radar and Wind Profiler Observations

ROBERT CIFELLI AND STEVEN A. RUTLEDGE

Department of Atmospheric Science, Colorado State University, Fort Collins, Colorado

DENNIS J. BOCCIPPIO

Center for Meteorology and Physical Oceanography, Massachusetts Institute of Technology, Cambridge, Massachusetts

THOMAS MATEJKA

Mesoscale Research Division, National Severe Storms Laboratory, NOAA, ERL, Boulder, Colorado

(Manuscript received 13 March 1996, in final form 15 April 1996)

ABSTRACT

Vertical motion profiles can be diagnosed with the mass continuity equation using horizontal divergence fields derived from various single-Doppler radar techniques such as EVAD (extended velocity–azimuth display), CEVAD (concurrent extended velocity–azimuth display), and VVP (volume velocity processing). These methods allow for the retrieval of mesoscale air motions in precipitating regions when the wind field is relatively homogeneous. In contrast, VHF wind profiler data can provide a direct measurement of vertical motion, albeit across a much smaller domain compared to the single-Doppler radar techniques. In this study, we compare horizontal divergence and vertical motion patterns derived from the various single-Doppler methods with those obtained from VHF profiler data.

The diagnosed profiles of horizontal divergence and vertical velocity from the single-Doppler (scanning radar) techniques are in qualitative agreement in the lower troposphere but often exhibit large variability at higher levels. Because of less stringent radar echo requirements, the VVP technique often analyzed data above the top of the EVAD–CEVAD analysis domain, resulting in a deeper layer of upper-level divergence. The CEVAD technique often produced a deeper and larger region of upward motion despite similar profiles of divergence, probably due to the CEVAD top boundary condition specification of particle terminal fall speed as opposed to the vertical air motion, as well as to the adjustment procedure employed during the regression solution.

The wind profiler data showed much larger vertical gradients and magnitudes of divergence and vertical velocity when averaged over the same time interval required to collect data for a single-Doppler retrieval. However, when all the available data were composited, the high-frequency variability in the wind profiler retrievals was reduced resulting in relatively good agreement between all analysis methods. The wind profiler usually sampled vertical motion (divergence) several kilometers above the single-Doppler retrievals, which the authors attribute to the stringent precipitation echo coverage requirements imposed by the scanning radar analysis techniques, thus limiting their vertical extent near echo top.

1. Introduction

Knowledge of vertical motions in mesoscale convective systems (MCSs) is important for understanding physical processes within these systems (e.g., precipitation production) as well as how these features interact with the large-scale environment through transports of heat, moisture, and momentum (Houze 1982; Johnson and Young 1983; Houze 1989). Diagnosed vertical velocities are also important for verification of numerical-model-derived kinematic, thermodynamic, and microphysical fields.

Numerous studies have discussed vertical motion profiles in the stratiform regions of MCSs (Zipser 1969; Gamache and Houze 1982; Johnson and Kriete 1982; Balsley et al. 1988; Houze 1989; Keenan and Rutledge 1993; and others). These studies have used a variety of techniques to diagnose the vertical motion profiles including single- and dual-Doppler techniques, wind profiler data to directly measure air motion, and rawinsonde data, which was used to calculate areal divergences with height, from which vertical motions were obtained after applying the mass continuity equation.

In this study we discuss and compare four techniques used to analyze vertical motions and horizontal diver-

Corresponding author address: Dr. Steven A. Rutledge, Department of Atmospheric Science, Colorado State University, Fort Collins, CO 80523-1371.
E-mail: rutledge@olympic.atmos.colostate.edu

gence patterns in the stratiform portions of MCSs. Three of the methods use scanning Doppler radar data and one uses vertically pointing VHF wind profiler data. Because the radar scanning strategy was less than ideal (discussed in section 2) and due to the different spatial scales sampled by the platforms (discussed in section 3), the emphasis is on examining the types of results one can expect when comparing divergence and vertical motion from different sensors using less than optimal designed scans. The scanning Doppler radar techniques are

- EVAD (extended velocity–azimuth display; Srivastava et al. 1986; Matejka and Srivastava 1991);
- CEVAD (concurrent extended velocity–azimuth display; Matejka 1993); and
- VVP (volume velocity processing; Waldteufel and Corbin 1979; Koscielny et al. 1982; Boccippio 1995).

In these three single-Doppler techniques, the kinematics of the mesoscale flow field is analyzed. The wind profiler technique, on the other hand, makes a direct measurement of vertical motion (Cifelli and Rutledge 1994). Both the Doppler radar and the wind profiler techniques require removing the effects of hydrometeor fall speeds. For the Doppler radar methods, these must be separated from the horizontal divergence, which can be integrated to produce an estimate of vertical air motion. For the profiler technique, fall speeds must be separated from the detected vertical velocity itself (Carter et al. 1991).

Each analysis technique has its strengths and weaknesses. The scanning Doppler radars provide an estimate of the mesoscale wind field within a relatively large volume and in short time. Because the scanning radar techniques are designed to analyze mesoscale flow patterns, the resulting horizontal divergence and vertical air velocity profiles appear smooth compared to those obtained from the wind profiler. However, for the scanning radar analyses to be performed, relatively large volumes filled with echo are required, limiting the situations in which the methods can be applied. The wind profiler, on the other hand, makes measurements over a relatively small spatial domain, enabling this technique to resolve small-scale variations in the vertical motion pattern. Unlike the microwave scanning radars, the profiler technique is also able to obtain these measurements in clear air. The resulting detailed vertical velocity structure is often rather complicated (and possibly noisy if the hydrometeor velocity signal is not easy to remove). Individual profiles may not be representative of the mesoscale flow. However, as we will show, the mesoscale vertical velocity pattern can be reclaimed by averaging the wind profiler retrievals in time. Thus, the wind profiler and scanning radar techniques are viewed as complementary.

Another disadvantage of the scanning radar techniques is that, since they retrieve vertical profiles of horizontal divergence, one or more boundary conditions must be specified before the mass continuity equation can be integrated to produce a profile of vertical air velocity w. These boundary condition assumptions can introduce error, especially in situations where data collection does not extend to a $w = 0$ level at the top of the cloud system. Such an effect would result when, for example, Doppler radar data are subject to significant attenuation or when upward motion extends beyond the minimum-detectable echo boundary. The profiler technique, by measuring w directly, avoids the need for specified boundary conditions.

EVAD was first used to diagnose upper-level ascent and lower-level descent of several tens of centimeters per second in the stratiform region of a midlatitude squall line (Srivastava et al. 1986). Further studies have utilized EVAD to examine the mesoscale structure in both tropical and midlatitude MCSs (Rutledge et al. 1988; Keenan and Rutledge 1993; and others). VVP has been applied to studies of the low-level kinematic wind field in clear air (Koscielny et al. 1982; Boccippio 1995) and to the study of tropical thunderstorm anvils (Boccippio 1995). CEVAD is a relatively new retrieval technique and the authors are not aware of a previous study in which this method has been examined in detail.

VHF wind profilers have been used to diagnose vertical motions in a variety of mesoscale precipitating systems occurring in the Tropics and midlatitudes. Balsley et al. (1988) presented air motions in clear air and precipitation conditions at Pohnpei Island (7°N, 157°E) in the tropical western Pacific using a vertically pointing wind profiler. Based on rainfall rates from a nearby rain gauge, Balsley et al. obtained composite profiles for both the convective and stratiform portions of the precipitating systems. Cifelli and Rutledge (1994) performed a similar analysis for MCSs occurring over the Maritime Continent region near Darwin, Northern Territory, Australia. Cifelli and Rutledge were able to extract the vertical air motions for different portions of precipitating systems that passed over a VHF wind profiler site during both the monsoon and monsoon break convective regimes.

Augustine and Zipser (1987) used a three-beam VHF wind profiler to study the horizontal wind structure within several midlatitude MCSs observed during PRE-STORM (Preliminary Regional Experiment for STORM-Central). The profiler-derived horizontal wind fields were found to be qualitatively consistent with wind fields derived from nearby rawinsondes. Moreover, Yoe et al. (1992) presented a more detailed analysis of the horizontal and vertical wind fields for one of the MCSs discussed in Augustine and Zipser (1987). Using data from a VHF profiler in conjunction with two 5-cm Doppler radars, Yoe et al. (1992) showed that the wind profiler was able to identify many of the storm mesoscale features (e.g., midlevel rear inflow jet; upper-level front-to-rear flow), similar to the

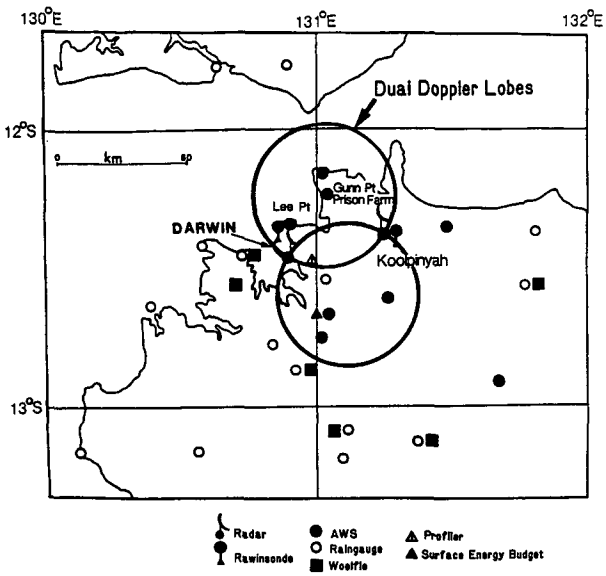

FIG. 1. Location of the observational network used during the DUNDEE field experiment. (Adapted from Rutledge et al. 1992).

scanning radars. A comparison of the vertical air motions diagnosed by profiler and scanning radars using a single-Doppler retrieval technique showed that the vertical velocity profiles were in reasonable agreement for most heights above the melting level (for the one analysis time presented in the study).

VHF profiler data have also been used to diagnose vertical motions in precipitating systems over Japan (Wakasugi et al. 1986; Wakasugi et al. 1987; Sato et al. 1990; Larsen et al. 1991). In particular, Larsen et al. (1991) used VHF wind profiler data to diagnose vertical motions using VAD (velocity–azimuth display) technique (discussed in section 2) as well as direct measurements of the clear air during a cold-frontal passage. Their study concluded that the methods agreed well in regions of isotropic scatter. However, poorer correlations were found in regions of strong stratification or anisotropic scattering (aspect sensitivity). Chilson et al. (1993) diagnosed the vertical air motion and precipitation fall speeds in a thunderstorm that passed over a VHF profiler site in Puerto Rico. In that study, collinear beams from UHF and VHF profilers were used to analyze the precipitation and wind structure of the thunderstorm.

Ralph et al. (1993) described the use of 50-MHz wind profiler data in conjunction with automated surface meteorological and rawinsonde data to resolve a ducted mesoscale gravity wave. The array of instrumentation in that study provided a mutually consistent picture of the detailed vertical structure of the wave from the ground level to just above a critical level.

To compare and contrast the EVAD, CEVAD, VVP, and profiler techniques, we examine vertical profiles of horizontal divergence and vertical air velocity in several tropical MCSs near Darwin, Northern Territory, Australia that were observed during DUNDEE (Down Under Doppler and Electricity Experiment; Rutledge et al. 1992). Section 2 provides a summary of the data collection methodology as well as a brief overview of each retrieval technique. The sampling scales of the wind profiler and scanning radar platforms are compared in section 3. Representative individual retrieval and composite results are presented in section 4. We interpret these results in light of the strengths and weaknesses of the four techniques used.

2. Methodology

The location of the MIT and TOGA radars and the Darwin 50-MHz wind profiler in DUNDEE are shown in Fig. 1. The wind profiler was located approximately along the baseline between the two 5-cm Doppler radars. The location of the observational network at the southern tip of the Maritime Continent (Ramage 1968) provided a unique opportunity to examine MCSs occurring during both the active monsoon (maritime) and the monsoon break (continental). In this study, data analyzed from the stratiform portion of four MCSs (three break and one monsoon) are presented.

Characteristics of the scanning radars and the wind profiler are shown in Table 1. The radar scanning strategy for the single-Doppler retrievals is summarized in Table 2. Radar elevation angles ranged from 1° to 45° (most of the time) or 1° to 60° (occasionally) and incorporated a total of 15–18 sweeps for each radar volume. Although this scan strategy was not ideal for the retrievals utilized in this study, it was necessary in order to satisfy all the radar sampling constraints of DUNDEE. More reliable results could probably be obtained if the radar scanned above 50° and included at least 20 sweeps in the radar volume (Matejka and Srivastava 1991).

As discussed below, each scanning radar retrieval method makes assumptions about the variability of the

TABLE 1. Characteristics of the MIT and TOGA microwave radars and the Darwin VHF wind profiler used during DUNDEE (adapted from Cifelli and Rutledge 1994).

Characteristic	MIT	TOGA	Wind profiler
Wavelength (cm)	5.4	5.3	600
Peak power (kW)	250	250	30
Pulse length (μs)	1.0	0.50, 1.9	6.7
Beamwidth (°)	1.4	1.65	3.4
Minimum detectable signal (dBm)	−106	−113	−165*
Pulse repetition frequency (s^{-1})	921	921	1000
Antenna gain (dB)	42.2	40.8	29.7
Number of gates	226	224	50
Polarization	Horizontal	Horizontal	Horizontal

* The minimum detectable signal of the VHF wind profiler has an estimated uncertainty of ±20 dB.

TABLE 2. Radar scan strategy for single-Doppler retrievals employed by the MIT and TOGA radars during the four DUNDEE events.

Scan number	MIT elevation tilt (°)	TOGA elevation tilt (°)	TOGA elevation tilt (°)*
1	0.8	0.8	0.8
2	2.5	2.4	2.5
3	4.2	4.0	4.0
4	5.9	5.6	5.4
5	8.0	7.2	6.8
6	10.0	8.8	8.3
7	12.0	11.0	10.0
8	15.0	13.0	12.1
9	18.0	15.0	14.3
10	21.0	17.0	17.3
11	25.0	20.0	20.8
12	29.0	23.0	25.0
13	33.0	26.0	30.0
14	38.0	30.0	35.0
15	45.0	35.0	40.0
16		40.0	50.0
17		45.0	55.0
18			60.0

* Scan strategy employed only during the 28 January 1990 event.

wind field across the analysis domain and the techniques are therefore best applied to precipitating regions where the wind field is relatively homogeneous (i.e., linear or quadratic variations can be assumed; Matejka and Srivastava 1991). A total of 22 radar volumes from the stratiform portion of the four MCSs were analyzed with each single-Doppler retrieval technique and a corresponding number using the wind profiler retrieval. The sample is admittedly small for comparison purposes; however, as shown in section 4b, the sample is sufficient to illustrate that the wind profiler and scanning radar techniques are complementary in the study of MCS kinematic structures.

The individual radar volume scans were first scrutinized in order to evaluate the suitability of the retrieval methods for each volume of data. Subsequent to processing, regression statistics from each method were evaluated to help flag spurious (bad) retrievals (Matejka and Srivastava 1991; Boccippio 1995). Also, the single-Doppler retrieved horizontal winds were compared to the nearby Darwin rawinsonde wind profile when available (Fig. 1) in order to check for consistency.

Independent validation of the wind field kinematic structure was available from dual-Doppler analyses performed on two of the events in this study. The dual-Doppler vertical motion results are presented in conjunction with the scanning radar retrievals in section 4 and are shown to be in good agreement with the scanning radar profiles.

Brief summaries of each of the four analysis methods follow.

a. EVAD analysis

The EVAD algorithm consists of two steps:

1) Traditional VAD (Browning and Wexler 1968) analysis, which analyzes horizontal rings of radial velocity data for each elevation cone within a specified vertical cylinder of radar data to determine the mean horizontal wind field; and

2) EVAD analysis, which separates the combined effect of divergence and precipitation fall speed from the VAD-derived horizontal wind field and calculates divergence, hydrometeor fall speed, hydrometeor terminal fall speed, and vertical velocity as a function of altitude within a specified volume of VAD data.

In VAD, the radar data are divided into horizontal rings centered on the radar and a truncated Fourier series is used to model the radial velocity field v_r according to

$$v_r = \sum_{i=1}^{7} a_i f_i(\phi) + \epsilon, \qquad (1)$$

where $f_1 = 1$, $f_2 = \sin\phi$, $f_3 = \cos\phi$, $f_4 = \sin 2\phi$, $f_5 = \cos 2\phi$, $f_6 = \sin 3\phi$, $f_7 = \cos 3\phi$, ϕ is azimuth angle, a_i represents the particular Fourier coefficient, and ϵ is the departure of the regression model from the actual observations (Matejka and Srivastava 1991). It is important to note that in the VAD analysis, reliable solutions for the Fourier coefficients (a_i) are typically obtained in situations where the wind field is relatively uniform (stratiform as opposed to convective portions of precipitating regions) and nearly complete echo coverage surrounds the radar.[1] In the ideal situation, the wind data are approximately evenly spaced around the radar so that the basis functions f_i in (1) form an orthogonal set and the regression is not particularly sensitive to departures from the model assumptions (Matejka and Srivastava 1991). The time required for the radar to complete an individual VAD volume scan was approximately 8–10 min.

In order to apply EVAD, it is assumed that both hydrometeor fall speed and divergence are horizontally uniform within a specified vertical layer. The depth of each layer is determined from the radar gate spacing (usually 500 m for the particular radar data used in this study) and is constant throughout the EVAD volume. Moreover, it is assumed that there are no significant temporal variations in the wind field during the radar volume sampling period.

For a given height interval containing multiple rings, both particle fall speed and divergence may be determined from a weighted least squares fit independently

[1] Matejka and Srivastava (1991) recommend that the EVAD technique be applied in situations where the largest azimuthal gap in radar echo coverage surrounding the radar is 30° or less.

in each layer (Srivastava et al. 1986; Matejka and Srivastava 1991; Matejka 1993), according to

$$\frac{2a_0}{r\cos(\alpha)} = D + W_P\frac{2\sin(\alpha)}{r\cos(\alpha)}, \qquad (2)$$

where D is horizontal divergence, W_P is hydrometeor vertical velocity ($w - V_t$; V_t is the hydrometeor terminal fall speed), a_0 is the VAD estimated zeroth Fourier coefficient, α is the elevation angle of the radar beam, and r is the radius of the analysis domain.

Vertical velocity within the EVAD analysis domain is calculated by integrating the anelastic form of the mass continuity equation. In order to account for errors accumulated in the integration, a variational method similar to that employed by O'Brien (1970) is used to obtain a modified profile of divergence [see Eqs. (21) and (22) of Matejka and Srivastava 1991].

The altitude of the highest echo from one of the three steepest elevation scans analyzed in VAD was utilized as the location of the EVAD top boundary and it was assumed that the vertical velocity at this point was zero. It was also assumed that the vertical velocity was zero at the altitude of the radar (essentially sea level). For the four MCSs we studied, the EVAD analysis domain radius was set at 30 km, which allowed for considerable overlap in data coverage between the MIT and TOGA radars when both systems were collecting simultaneous data (Fig. 1).

b. CEVAD analysis

CEVAD is identical to EVAD except for two important aspects. In CEVAD, the solution is obtained by an optimization of (2) throughout all the layers concurrently, not independently as for EVAD (Matejka 1993). Therefore, the boundary conditions at the top and bottom of the cylinder are satisfied automatically during the solution of the profile of D itself. In addition, the top boundary condition is formulated in terms of a specified V_t. Thus, since $w = W_P + V_t$ at the top, and since W_P itself is solved for, w at the top is not an inflexible specified condition; rather, w at the top boundary is allowed to respond to the data in the entire column. More importantly, imposing V_t rather than w as the top boundary condition is more appropriate in situations where the radar echo does not extend close to cloud top. The variational adjustment of the divergence profile in CEVAD is incorporated into the concurrent optimization of (2) rather than imposed subsequently as in EVAD (Matejka 1993).

Sensitivity analyses were performed on the selection of terminal fall speed values at the upper boundary in all radar volumes using the CEVAD technique. Fall speeds were varied from 0.5 to 2.0 m s^{-1} and, in general, the results were not particularly sensitive to the value selected. Therefore, for comparison purposes, a terminal fall speed value of 1.0 m s^{-1} was chosen as the upper boundary condition in all of the radar volumes analyzed with CEVAD.

c. VVP analysis

The VVP method assumes that the wind field varies linearly around its value at a given point (Waldteufel and Corbin 1979; Boccippio 1995). The radial wind field $\mathbf{v}_r$ is modeled according to

$$\mathbf{v}_r = \sum_{k=1}^{9} m_k p_k + \boldsymbol{\epsilon}, \qquad (3)$$

where p_k represents a set of wind field components and their spatial derivatives and m_k are the geometric coefficients (basis functions). One fundamental difference between the VVP and VAD formulations is that in VVP, one chooses the wind field parameters to retrieve from the radar data and then determines the corresponding basis functions to create the regression model (Boccippio 1995). In contrast, the VAD method selects basis functions and derives wind components from the regressed parameters. As discussed in Boccippio (1995), an optimal set of parameters to retain in the VVP model is the basic state wind field and the horizontal shear terms.

The VVP is typically applied to thin layers of data (i.e., 250–500 m) at successive heights to provide a vertical profile of retrieved parameters. Regression diagnostics are used to filter (mask) unsuitable retrievals from the analysis domain and to define an acceptable upper boundary for divergence integration. Missing data is then filled by a kriging technique (Boccippio 1995). The top of the analysis domain is chosen as the highest level where at least 300 data points contribute to the regression in the top layer and both divergence and vertical motion are set to zero at this level.

Similar to EVAD, the VVP method is sensitive to analysis errors in regions of large gaps in radar echo coverage. However, there is a philosophical difference between VVP and VAD in the treatment of echo gaps surrounding the radar. Mathematically, given assumptions about the complexity of the wind field and its deviations from an assumed model, a certain acceptable gap size can be determined. This is the approach used in VVP. Boccippio (1995) has shown that the sensitivity to echo gap coverage appears to be principally a consequence of neglecting unretrievable horizontal curvature terms in the regression model. Moreover, diagnostic analysis suggests that the VVP method performs reasonably well for radar echo gaps ranging up to 90° in precipitating regions when the horizontal curvature is less than $O(10^{-8}\ \mathrm{m^{-1}\ s^{-1}})$. However, in a few trials performed on precipitating systems, Matejka and Srivastava (1991) found that VAD retrievals often performed poorly when the gap size was greater than 30°. This led the authors to conclude that the discrepancy of the wind field in the gap from that in the echo was

probably larger than that assumed in the mathematical treatment. In other words, the wind kinematics in the gap were not necessarily predictable from the wind kinematics in the echo regions. The conclusion is that, in either retrieval method (i.e., VAD or VVP), the results must be interpreted cautiously in situations where the techniques are applied in regions containing nonuniform echo.

d. Wind profiler analysis

A description of the technique utilized to calculate vertical motion from wind profiler data can be found in Cifelli and Rutledge (1994). Briefly, the Darwin profiler operated with a single beam at vertical incidence during the 1989–90 DUNDEE field season. At 50 MHz, the profiler can detect both turbulence (i.e., clear air) and precipitation fall speed echoes directly (Carter et al. 1991). Each profiler observation had a temporal resolution of 100 s and a gate spacing of 495 m. Prior to extracting vertical velocity, the raw spectra were averaged in time to reduce random noise fluctuations and to improve the statistical significance of the results. The length of the averaging time was 10 min, the approximate length of time required to perform a single-Doppler radar volume scan.

Cifelli and Rutledge (1994) used a combination of methods to separate the vertical velocity and precipitation components in the averaged Doppler spectra. First, an objective algorithm to derive both atmospheric turbulence and precipitation parameters was developed based on the method described by Sato et al. (1990). The Sato et al. technique utilizes a Marshall–Palmer distribution to approximate the precipitation component of the spectra and a Gaussian distribution to fit the turbulence component to the observed Doppler spectrum $S(v)$ according to

$$S(v) = S_t(v) + S_p(v) * S_0(v) + P_n, \qquad (4)$$

where $S_t(v)$ represents the Doppler power at frequency v associated with backscatter from irregularities in the refractive index due to turbulence, $S_p(v)$ represents the Doppler spectrum due to precipitation, $S_0(v)$ is a normalized form of $S_t(v)$, P_n represents the noise level in the Doppler spectrum and the symbol "*" denotes the convolution operation (Sato et al. 1990).

Sensitivity analysis with the curve-matching program showed that the algorithm fit the spectra reasonably well below the melting level (~4.7 km) and above about 9 km; however, in the region between about 4.5 and 9.0 km, the program was often unable to distinguish between the vertical velocity and precipitation components. This was probably due to the existence of water drops, snow, and other types of ice particles in the mixed-phase region of the cloud with fall speeds comparable to the vertical air motions (Carter et al. 1991). Because of the wide range of hydrometeor fall speeds, the precipitation and vertical velocity components of the spectra "merged together" to the point that the curve-fit program attempted to fit both parts of the spectra with a single Gaussian curve (i.e., the fit was underdetermined). In situations where the components of the spectra could not be objectively separated, a second analysis technique was used to extract the vertical velocity information from the spectra. In these cases, the center of the Gaussian was manually edited so that the mean vertical motion coincided with the approximate location of the turbulence peak power (Cifelli and Rutledge 1994).

An arbitrary signal-to-noise ratio was developed in this study in order to determine if the power return at a particular gate represented a meteorologically significant signal or was part of the noise spectrum. If the ratio of log(signal power)/log(noise power) determined by the curve fitting algorithm was below 1.2, it was assumed that the power return was insignificant and no vertical velocity value was recorded for that particular gate. The value of 1.2 was often found to be approximately coincident with the location of cloud-top height, based on available GMS satellite imagery.

Horizontal divergence was calculated from the wind profiler vertical motion data through a centered-difference calculation of the anelastic continuity equation, using a density profile generated for each MCS based on the 1200 UTC Darwin sounding for that day. Inspection of the raw divergence profiles showed a significant amount of high-frequency variability (noise) in the vertical. Therefore, a three-point low-pass statistical filter was applied to the wind profiler vertical velocity data prior to the centered-difference calculation, in order to smooth the resulting divergence estimate. The filter response chosen preserved 75% of features with a wavelength of at least 3.7 km and 25% of features with a wavelength of at least 1.8 km. Note that the differencing procedure had the effect of slightly stretching the upper boundary of the divergence profile one half a grid level (i.e., 247 m) above the corresponding vertical motion top boundary.

3. Sampling geometry and the effects of averaging

In order to place the wind profiler and single-Doppler radar results in proper context, it is necessary to examine the sampling dimensions of each instrument. For a vertically pointing wind profiler in a region of relatively small vertical wind shear, the volume of atmosphere sampled by the profiler beam is conical with horizontal dimensions proportional to the profiler beamwidth. Because of the dwell time and averaging process described in section 2c, the geometry of the profiler sampling region at any given height becomes elliptical, with increasing eccentricity as the length of the averaging interval increases and/or the convective system advection speed increases. The major axis of the ellipse is parallel to the direction of storm motion (see Fig. 2 and Table 3). Note that the orientation of

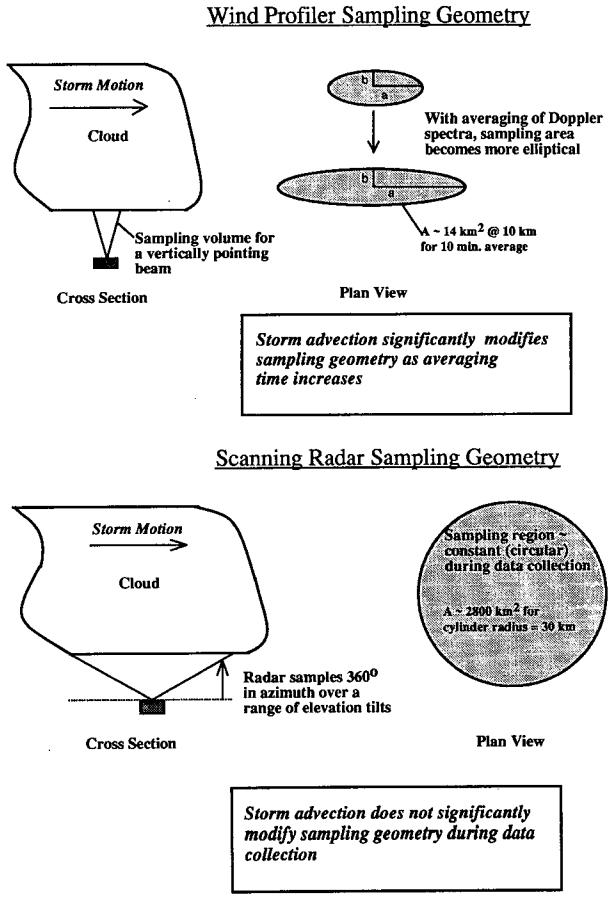

FIG. 2. Schematic diagram showing the sampling geometry and area of the 50-MHz wind profiler (top) and the 5-cm Doppler radars (bottom).

the ellipse can vary with height in regions containing large vertical shear of the horizontal wind (e.g., in an MCS with intense storm relative flow).

In contrast, the 5-cm radars collected data by scanning the beam through 360° of azimuth over a range of elevation angles. Assuming nearly continuous radar echo coverage around the radar, the sampling volume for any of the single-Doppler retrieval techniques is cylindrical, so that at any given height, the sampling area is approximately constant (circular).[2] For a cylinder with radius 30 km, the total sampling area is about 2800 km^2. In contrast, the wind profiler samples only a small fraction of this area at any given height (Table 3). The results in Table 3 indicate that any comparison of kinematic structures between the two platforms will have to account for the large differences in spatial sampling. In this study, the sampling timescales have at least been made similar; nevertheless, we emphasize that the atmospheric volume sampled by each platform is quite distinct, even when the profiler data are averaged over a relatively long sampling period. This fact should be kept in mind when interpreting the results in section 4.

For a volume of atmosphere that is sampled by the wind profiler and radar at the same time but different spatial scales, we may attribute differences in the diagnosed fields to some combination of the following:

(a) biases in the wind profiler data resulting from contamination of the precipitation component of the Doppler spectra with the turbulence component of the spectra [contamination by precipitation will introduce a negative (downward) bias in the profiler vertical velocity estimates];

(b) errors due to the evolution of the divergence and vertical velocity fields during the sampling period;

(c) application of an inappropriate top boundary condition for single-Doppler retrieval analysis; and

(d) nonhomogeneities in the horizontal divergence and vertical velocity fields across the analysis domain (differences in the region sampled by the profiler and the single-Doppler radars)—the meteorologically significant variability.

As discussed in Cifelli and Rutledge (1994), the vertical air motion component of the VHF wind profiler spectra obtained in the MCSs they studied were susceptible to precipitation contamination in the mixed-phase region of the cloud. In particular, the majority of the bias in the stratiform portion was evident in the elevation range of 3.5–6.5 km of each MCS. In this altitude range, air motion estimates were shifted over 2 m s^{-1} on average to correct for the effects of precipitation (Cifelli and Rutledge 1994). Although the wind profiler vertical motion estimates were adjusted to account for precipitation bias, we cannot rule out the possibility that the vertical velocity estimates have considerable error in some of the range gates. We note that the VVP retrievals typically showed a 1.5–2-fold increase in the horizontal wind rmse (root-mean-square error) in this same altitude range, suggesting either fall speed or vertical motion anomalies at these heights.

In regard to potential errors resulting from the evolution of divergence and vertical motion fields during sampling [see (b) above], Cifelli and Rutledge (1994) showed that the wind profiler vertical motion (divergence) fields in the stratiform portions of the convective systems they studied were relatively stable for averaging periods of 5–15 min. It was not possible to perform a similar sensitivity study for the scanning radar data since the sampling period was fixed. However, retrievals that could be performed at consecutive (10

[2] During the time required to collect a complete volume of radar data (8–10 min), the radar sampling region is modified as described above for the wind profiler. However, in the case of the scanning radar, the change in sampling geometry during data collection is relatively small, due to the large region of atmosphere sampled by the radar relative to the storm advection speed (Matejka and Srivastava 1991).

TABLE 3. Sampling area calculations for the wind profiler compared to the single-Doppler radar. The calculations are performed for an arbitrary height of 10 km and assume a storm speed of 10 m s^{-1} over the profiler (parallel to the major axis a). Note that the profiler area is an ellipse with increasing eccentricity (major axis length) as the averaging time increases (see Fig. 2). We assume that the single-Doppler sampling domain is approximately cylindrical with a radius of 30 km so that the area at any height is constant.

Avg. interval (min)	Major axis a (km)	Minor axis b (km)	Profiler sampling area πab (km^2)	Radar sampling area πr^2 (km^2)	Fraction of radar area (%)
5	4.6	0.6	8.7	2827	~0.3
10	7.6	0.6	14.3	2827	~0.5
15	10.6	0.6	20.0	2827	~0.7
30	19.6	0.6	36.9	2827	~1.3
100	61.6	0.6	116.1	2827	~4.1

min) intervals showed little difference in the diagnosed profiles, suggesting that the kinematic fields did not evolve appreciably during sampling (at least at vertical spatial scales measured by the radar: 0.5–1.0 km).

Potential error source (c) and the scale-difference effect (d) above are discussed in section 4. We simply note here that it is difficult to directly compare the kinematic structures diagnosed from each observation platform, not only due to potential errors in the analysis methods, but also due to the large variability in the wind profiler estimates of vertical motion resulting from small-scale turbulence features.

4. Results

a. Selected vertical profiles using radar and wind profiler analyses

Selected horizontal divergence and vertical velocity results diagnosed using single-Doppler radar techniques (EVAD, CEVAD, and VVP) and the wind profiler for four MCSs are presented in this section. Each profile is representative of an 8–10-min time period during the passage of the MCS over the observational network.

When comparing the vertical motion and horizontal divergence results, it is important to remember a fundamental distinction in the kinematic quantities measured and diagnosed with the scanning radar and wind profiler platforms. With regard to the scanning radar, divergence is the quantity that is directly measured (i.e., retrieved) and vertical motion is derived through an integration procedure. In contrast, the primary measured quantity of the wind profiler is vertical motion and divergence is diagnosed by differentiation of the measured vertical motion field. Since derivatives of a measured quantity tend to amplify existing fluctuations (e.g., errors), the wind profiler divergence estimates can appear noisy compared with their vertical motion counterparts, even when the data are filtered.

Representative profiles of horizontal divergence and vertical motion for each of the four MCSs are shown in Figs. 3 and 4, respectively. With the exception of the 12 January 1990 monsoon MCS, all of the scanning radar profiles in Fig. 3 show a convergence peak in the vicinity of the melting level with weak divergence below about 4 km, consistent with the structure observed in midlatitude and tropical MCSs (Gamache and Houze 1982; Rutledge 1991; Biggerstaff and Houze 1993; Brandes and Ziegler 1993; Mapes and Houze 1993; Cifelli et al. 1994, and others). This lower tropospheric divergence pattern generally corresponds to downward motion with a peak near 3–4 km (Fig. 4). Also, with the exception of the 22 January 1990 plot, the scanning radar profiles show convergence extending from about 4 to at least 8 km, which corresponds to mostly downward vertical motion in the EVAD and VVP profiles (Fig. 4). The shallow layer of upper-level divergence (completely absent in the 5 December 1989 EVAD and CEVAD retrievals) in these DUNDEE MCSs is somewhat anomalous compared to many of the previous studies cited above. As discussed below, the apparent lack of upper-level divergence was at least partially due to insufficient echo near the top. This shows the weakness of using VVP and EVAD with $w = 0$ at the top boundary. More complete scanning at high elevations might have enabled sufficient echo coverage to be obtained at the high levels.

The EVAD technique for 5 December 1989 diagnosed convergence from about 4 km to the top of the profile (Fig. 3a). This pattern was noted in many of the volume scans analyzed with EVAD for this MCS and, as noted above, was due to the existence of nonuniform ("ragged") echo coverage in the upper portions of the stratiform cloud. Because of VAD's strict echo coverage requirement, the analysis could not be performed in the upper region of the cloud, below the base of the upper-level divergence region expected from the detrained anvil. Thus, the profile shows downward motion throughout the depth of the analysis column, which is an artifact of setting the vertical velocity to zero in a position well below cloud top.

Note that in three out of the four cases shown in Fig. 4, the CEVAD profile shows deeper and larger ascent compared to EVAD, despite similar divergence profiles. This situation occurred in the majority of radar volumes processed and is a consequence of the fact that

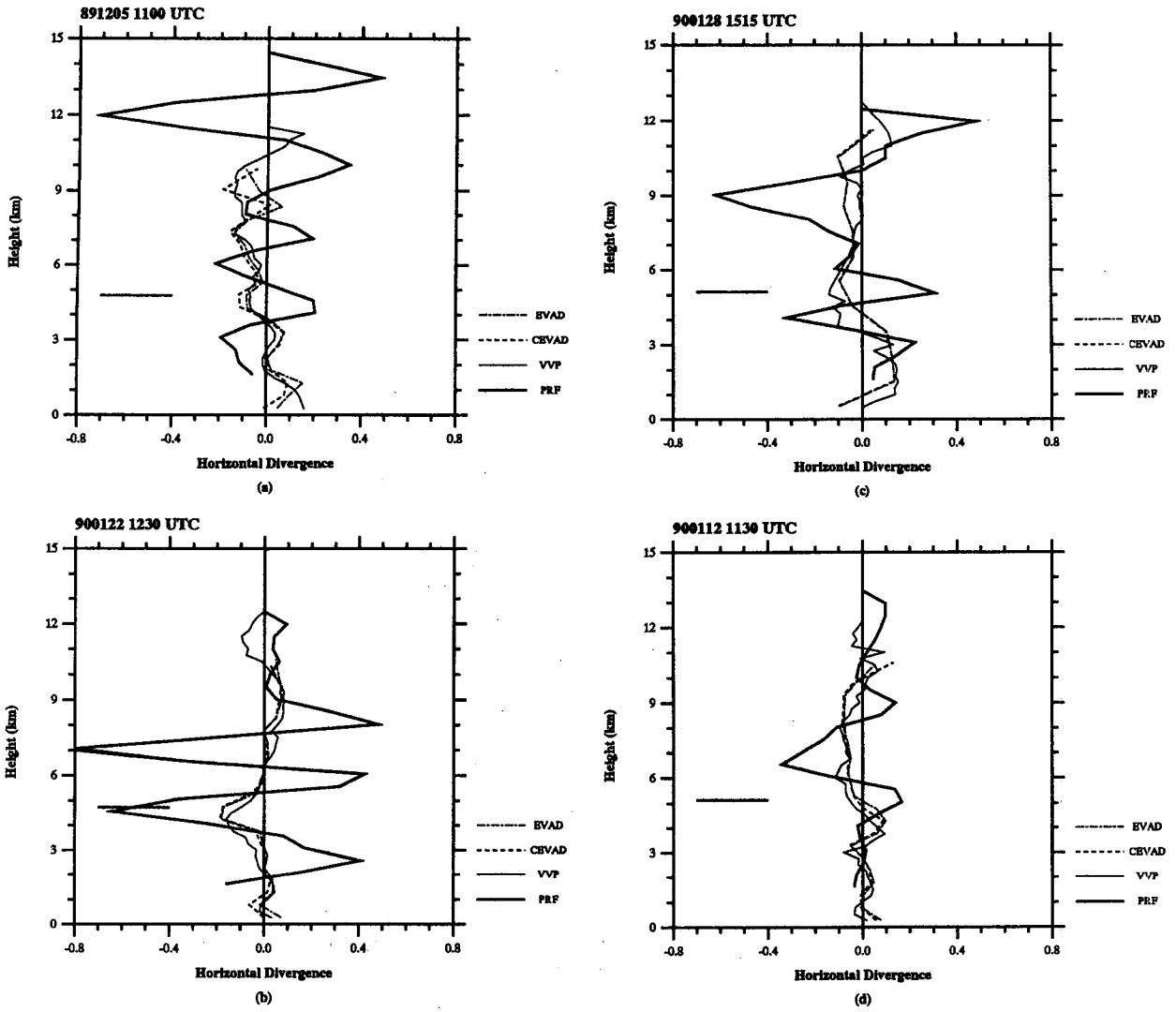

FIG. 3. Horizontal divergence profiles (10^{-4} s^{-1}) from the wind profiler and EVAD, CEVAD, and VVP single-Doppler techniques. Dates and analysis times are shown at the top of each plot and the line types corresponding to each analysis method are shown in the lower right portion of each plot. The horizontal line in the left portion of each plot shows the approximate location of the 0°C isotherm. The single-Doppler retrievals in (a), (b), and (d) were diagnosed from MIT radar data, while (c) was diagnosed with TOGA radar data.

CEVAD method does not inappropriately constrain the vertical velocity to zero at the top of the analysis domains (see section 4b).

For the 22 January 1990 break regime case, the scanning radar profiles show a crossover to divergence near 6 km with a corresponding updraft above the melting level (Figs. 3b and 4b, respectively), consistent with the conceptual model of stratiform vertical motion profiles discussed by Houze (1989). The VVP technique in this case diagnosed convergence (subsidence) above the EVAD and CEVAD analyses domains. The diagnosed convergence feature in the upper region of the VVP analysis domain is coincident with a relatively large shear layer in the observed upper-level radial velocity pattern (not shown). In this case, the retrieved upper-level convergence may be due to the proximity of the transition zone to the analysis domain. As documented by Heymsfield and Schotz (1985) and others, upper-level subsidence can occur to the rear of the MCS convective line in response to the interaction of outflow from the convective region with the environmental flow. The downdraft peaks in the 12 January 1990 monsoon case (Fig. 4d) are situated somewhat higher than the other break regime profiles. The single-Doppler vertical motion profiles for 12 January 1990 and 22 January 1990 are in good qualitative agreement with similar profiles derived from dual-Doppler analysis for these MCSs (Figs. 4b and 4d).

The wind profiler shows much larger gradients and magnitudes of divergence and vertical motion com-

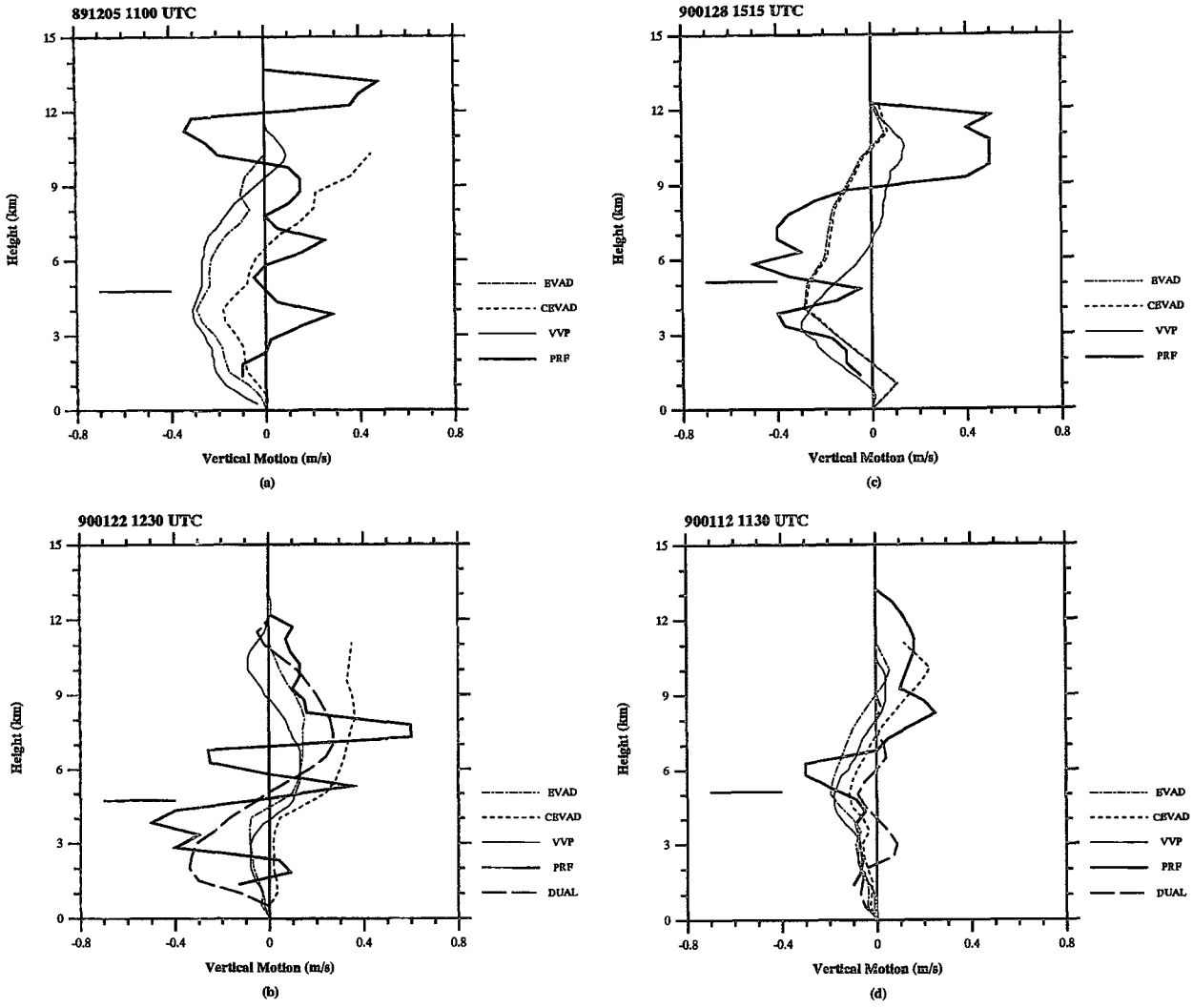

FIG. 4. Same as Fig. 3 except showing vertical motion (m s^{-1}). Dual-Doppler results, referred to as DUAL in the plot legend, are included for comparison in (b) and (d) (adapted from Keenan and Rutledge 1993).

pared to the single-Doppler retrievals (Figs. 3 and 4). The high-frequency variability in the wind profiler plots probably reflect the occurrence of convective scale drafts not resolved in the single-Doppler techniques. However, detailed comparisons of divergence and vertical motion between the wind profiler and the single-Doppler retrievals are complicated by the large variance in the profiler vertical motion estimates (see below). Note that the wind profiler diagnosed divergence in the vicinity of the melting level in three out of the four profiles, in contrast to the single-Doppler profiles (Fig. 3), which indicated convergence in all four cases.[3] The vertical oscillations of the profiler divergence measurements are similar to vertical reverberations observed in Pacific warm pool MCSs (Mapes and Houze 1995). Mapes and Houze suggest that oscillations may be produced by melting induced convergence in the MCS and the resulting excitation of a high-wavenumber internal mode. The vertical velocity profiles also indicate that the wind profiler was able to sample vertical motion a significant distance above the top of the single-Doppler analysis domain. A more detailed discussion of the differences in upper boundary locations is provided in section 4c.

Standard errors for the wind profiler vertical velocity estimates corresponding to Fig. 4 are shown in Fig. 5. Standard error profiles for the EVAD, CEVAD, and VVP retrievals are not included in Fig. 5, since analytical methods used to calculate this statistic must assume that the regression models are correct (i.e., no bias from neglected wind field components) and that

[3] In this sense, the wind profiler divergence profiles in Fig. 3 are atypical since the majority of the wind profiler results indicated convergence at the melting level, as described in section 4b.

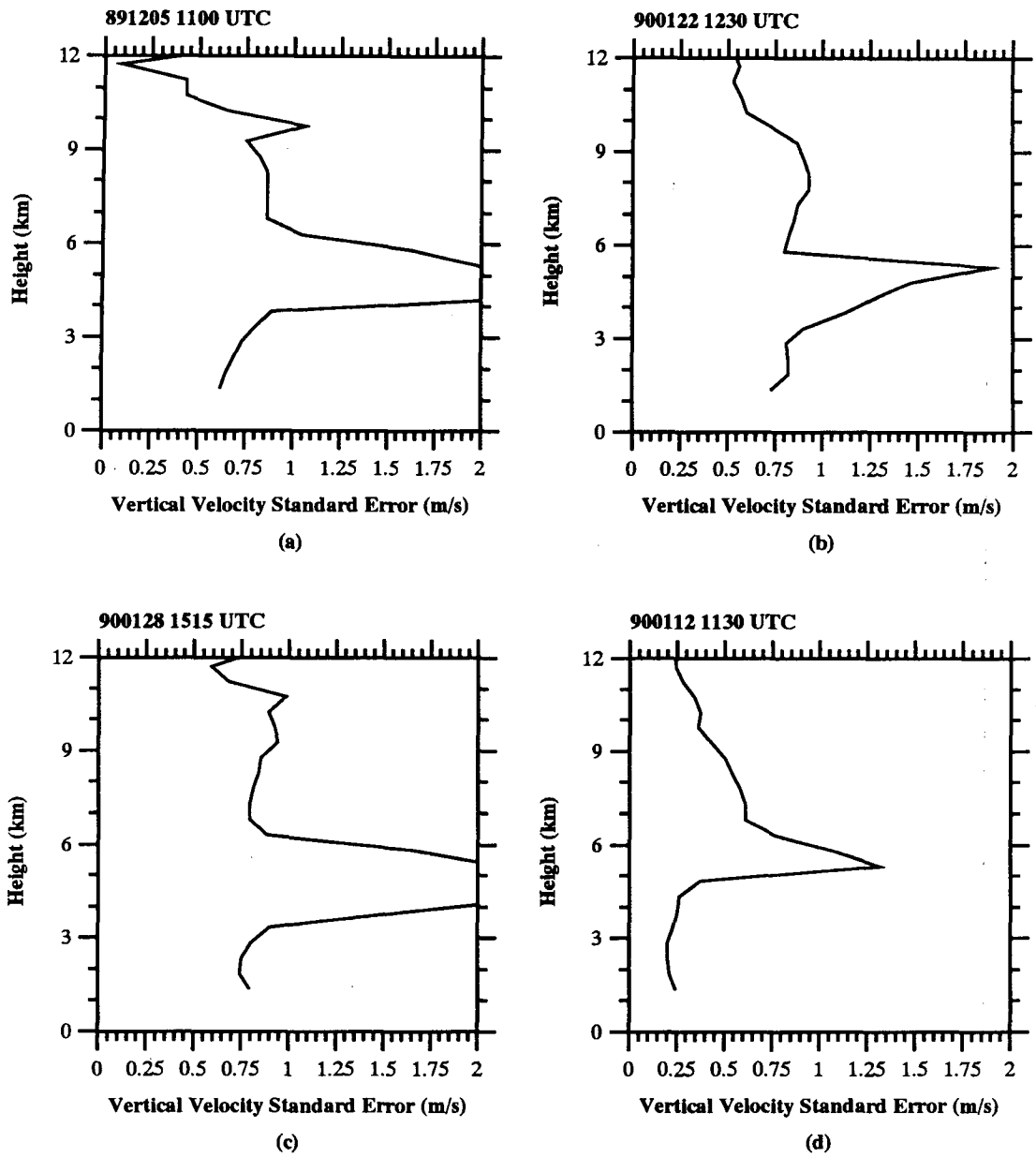

FIG. 5. Vertical motion standard errors estimates (m s^{-1}) for the wind profiler retrieval. Standard errors correspond to vertical velocity values in Fig. 4.

there are no errors in the top or bottom boundary condition (Matejka and Srivastava 1991).

The wind profiler standard error profiles shown in Fig. 5 must be interpreted cautiously, since the errors can be biased in regions where the precipitation and air motion components of the Doppler spectra were merged (see discussion in section 2d). In these situations, the curve-matching algorithm usually generated a single curve fit across the combined width of both spectra components (Cifelli and Rutledge 1994). This effect is particularly evident in the region from about 3.5 to 6.5 km where the wind profiler standard errors are enhanced (Fig. 5) because of limited separation between the clear air and precipitation Doppler spectra. Standard errors in this region are therefore not representative of the air motion alone.

The profiles in Fig. 5 show that uncertainty in the wind profiler vertical motion estimates are on the order of (or larger than) the mean values. The large variance of vertical motion is not surprising, given small spatial resolution and resulting turbulence gradients sampled by the profiler. In contrast, the model assumptions of

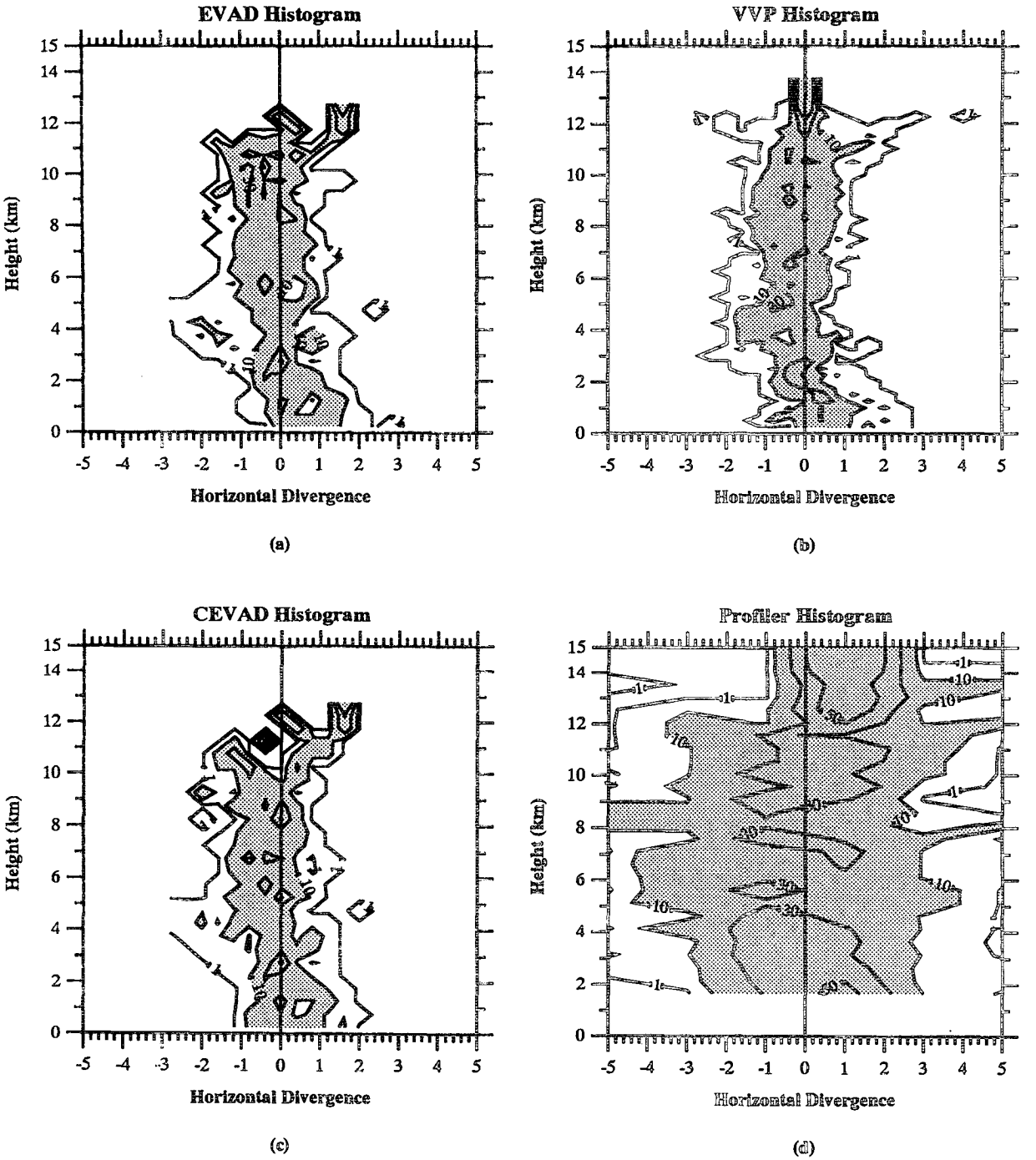

FIG. 6. Histogram profiles [i.e., CFAD (contoured frequency by altitude diagram); Yuter and Houze 1995] of composite horizontal divergence (10^{-4} s^{-1}) for the (a) EVAD, (b) VVP, (c) CEVAD, and (d) wind profiler retrieval techniques based on the 22 individual profiles. These plots show the horizontal divergence relative frequency of occurrence (%) as a function of height. Relative frequency of occurrence is contoured at intervals of 1%, 10%, 30%, and 50% with shading for values of at least 10%.

the single-Doppler retrievals prevent these methods from resolving small (submesoscale) features. The profiles in Fig. 5 illustrate an important point regarding the comparison of the single-Doppler and wind profiler vertical velocity estimates in Fig. 4: the single-Doppler vertical motion values are within the standard error of the wind profiler values at all heights. Thus, it is not possible to quantify differences between the radar and

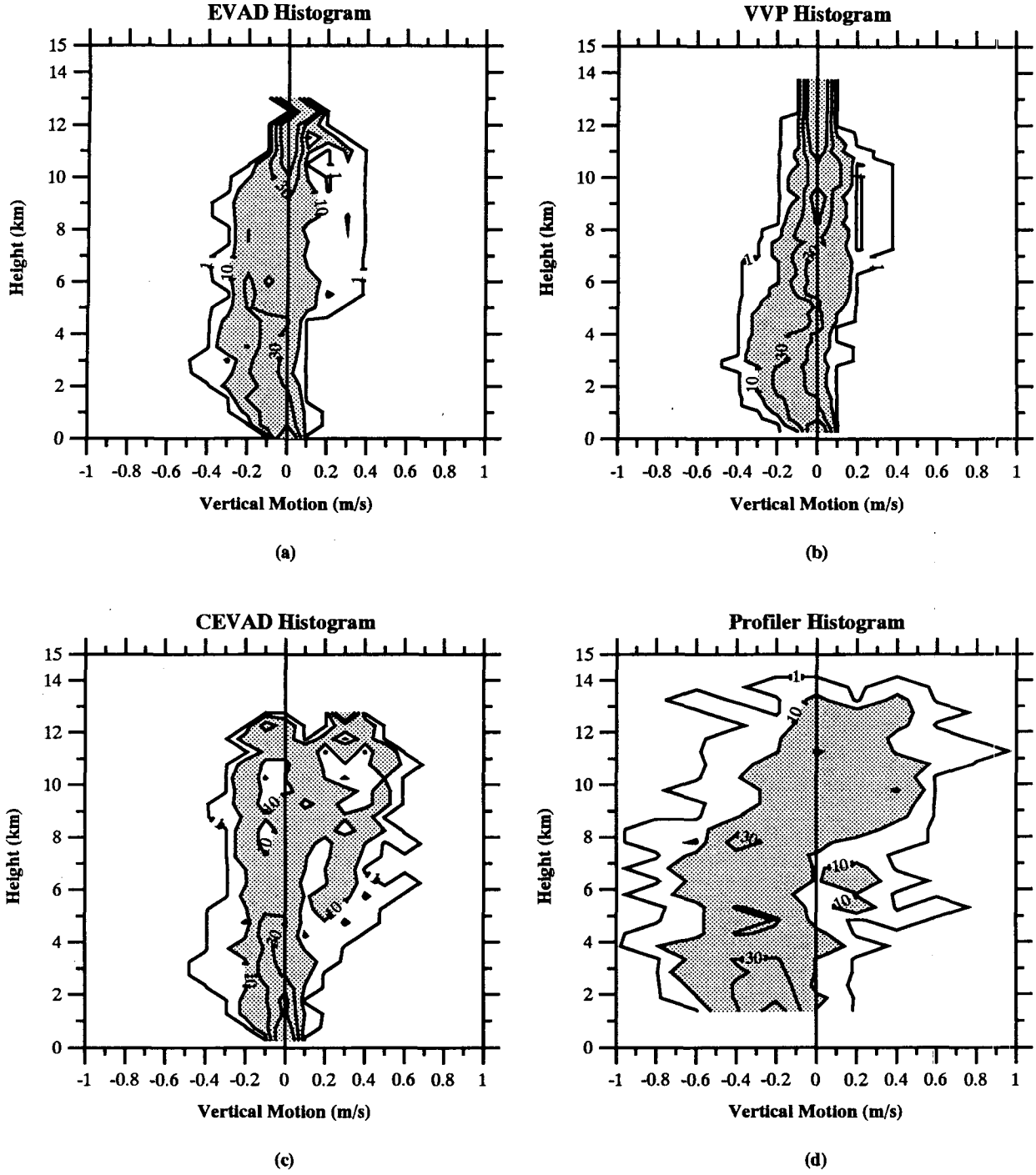

FIG. 7. Same as Fig. 6 except for vertical motion (m s^{-1}).

wind profiler vertical motion estimates. Note that the wind profiler standard errors in the monsoon case (Fig. 5d) are significantly less than in the break cases, reflecting weaker gradients of turbulence with associated smaller variability of the vertical velocity estimates.

b. Radar and wind profiler stratiform composite comparison

Composite profiles of horizontal divergence and vertical motion based on all 22 retrievals from the four

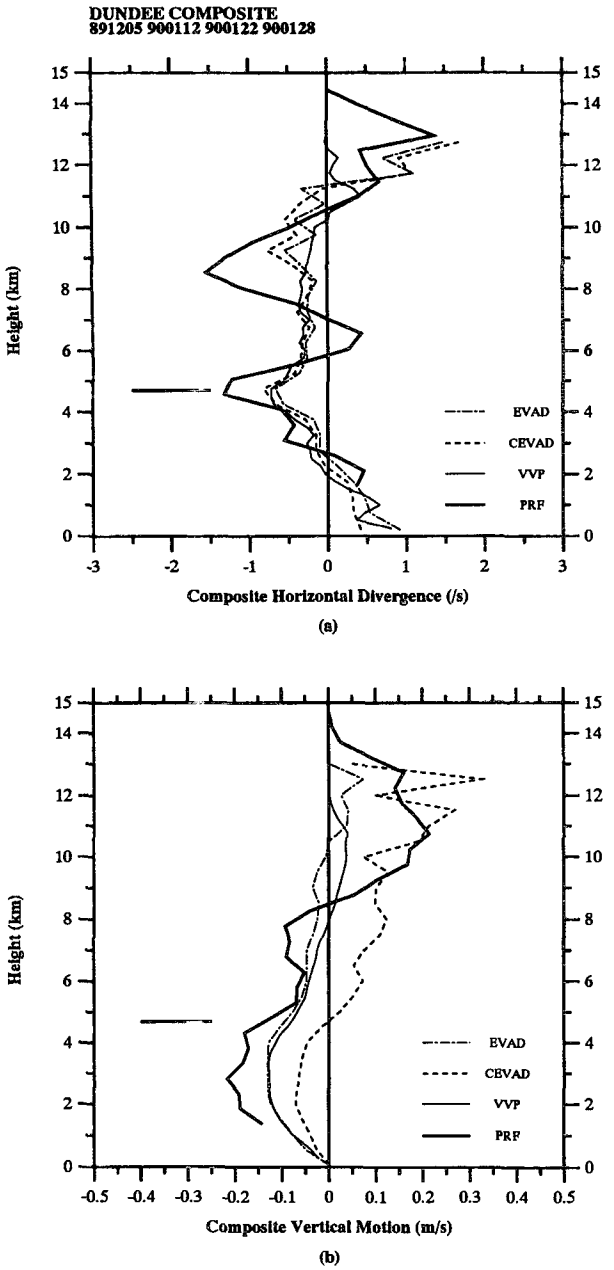

FIG. 8. (a) Composite mean horizontal divergence (10^{-4} s^{-1}) and (b) vertical motion (m s^{-1}) profiles for the wind profiler, EVAD, CEVAD, and VVP single-Doppler retrievals. Line type corresponding to each analysis method is shown in the lower right portion of each plot. The composites were constructed from a total of 22 individual profiles for each method.

MCSs are discussed in this section. The results are first presented in histogram profile [i.e., CFAD (contoured frequency by altitude diagram); Yuter and Houze 1995] format in order to compare the distributions for each retrieval method. Composite mean profiles are then shown in order to facilitate comparison to previous studies.

Histogram profiles of the composite divergence and vertical motion results for each retrieval technique are shown in Figs. 6 and 7, respectively. The contours in these plots represent the relative frequency of occurrence of the divergence and vertical motion estimates, respectively, as a function of height. The advantage of this sort of display is that the entire distribution for each technique may be examined as opposed to just the mean and standard deviation (Figs. 8 and 9, respectively). As Fig. 6 shows, all three of the single-Doppler retrievals have similar divergence distributions. In particular, the EVAD and CEVAD histogram profiles (Figs. 6a,c) are nearly identical, with the majority of each distribution showing midlevel convergence situated between upper- and lower-level divergence. The VVP divergence distribution (Fig. 6b) shows a somewhat higher frequency of divergence greater than 1×10^{-4} s^{-1} between 8 and 11 km compared to EVAD and CEVAD.

The single-Doppler divergence distributions are much narrower than the corresponding wind profiler histogram (Fig. 6d), although the overall patterns are similar. The difference reflects not only the small-scale variations sampled by the wind profiler compared to the scanning radar, but also the fact that the wind profiler divergence must be differentiated from the retrieved vertical motion field. As noted in section 4a, this procedure tends to amplify the existing variability, hence producing a relatively wide distribution.

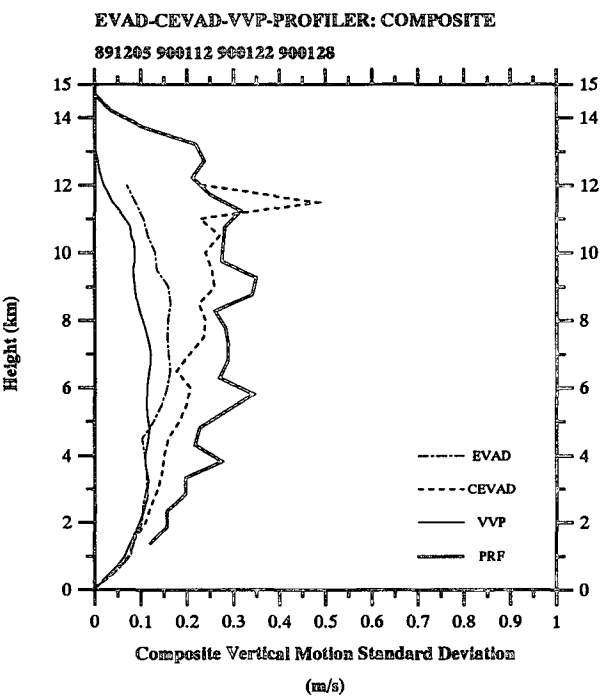

FIG. 9. Composite vertical velocity standard deviation (m s^{-1}) for each of the analysis methods corresponding to Fig. 8. Line type corresponding to each analysis method is shown in the lower right portion of each plot.

The EVAD and VVP vertical motion histogram profiles (Figs. 7a,b) are both relatively narrow with 10% or more of the values occurring between about -0.35 and 0.3 m s^{-1} at all heights. Perhaps the largest difference is the more frequent occurrences of deep downward motion in the EVAD profile. The EVAD distribution is biased by individual profiles which did not sample divergence in the upper portion of the analysis domain and subsequently produced a column integrated downward vertical motion pattern (recall discussion in section 4a). In contrast, the VVP histogram profile indicates a more common occurrence of upward motion above about 7 km (Fig. 7b). Because of the kriging technique employed in the postregression analysis stage, the VVP method does not require the nearly complete echo coverage pattern as in EVAD, and the VVP method was able to capture upper-level divergence in conditions of ragged echo coverage near radar echo top more often than EVAD; hence, VVP more commonly produced ascent in the middle to upper troposphere.

The CEVAD vertical motion histogram profile (Fig. 7c) is wider than either EVAD or VVP, especially in the middle to upper troposphere, reflecting the more common occurrence of relatively large vertical velocities (i.e., >0.2 m s^{-1}) diagnosed with this technique. As stated in section 4a, the CEVAD vertical velocity is not forced to zero at the top of the analysis domain. Thus, different divergence profiles can yield a wide range of vertical velocity values for a given terminal fall speed condition. The wind profiler histogram profile (Fig. 7d) is again wider than any of the single-Doppler distributions with the largest updraft velocities (approaching 1 m s^{-1}) occurring in the upper troposphere.

Composite mean profiles of divergence and vertical motion are shown in Fig. 8. The single-Doppler horizontal divergence composites all show a similar pattern with low-level divergence below about 2.5 km, a broad region of middle-level convergence extending to near 11 km and upper-level divergence to the top of the profiles (Fig. 8a). There is a small convergence peak centered near the melting layer at about 4.7 km in all of the composite profiles, consistent with negative buoyancy forcing at the melting level. The low-level divergence–middle- to upper-level convergence structure is similar to the stratiform divergence composite derived from aircraft radar data by Mapes and Houze (1993; their Fig. 7) in monsoon MCSs sampled off the coast of northern Australia during EMEX (Equatorial Mesoscale Experiment). The DUNDEE composite indicates that the crossover from low-level divergence to convergence occurs about 1 km lower, on average, than in the EMEX composite analysis of Mapes and Houze (1993). Given the width of the DUNDEE divergence distributions (Fig. 6) and the difference in sample sizes between the EMEX and DUNDEE composites (22 DUNDEE vs 37 EMEX), it is difficult to determine the extent to which differences in the crossover level are meteorologically significant. Nevertheless, it is possible that the difference in the profiles may be due to the fact that the DUNDEE composite is biased toward the continental convection regime (three out of four systems studied occurred during the monsoon break) compared to the monsoon (oceanic) regime MCSs sampled during EMEX, as well as the subjectivity in defining the stratiform precipitation portion of the MCSs. Perhaps the largest difference between the EMEX and DUNDEE composites is the occurrence of upper-level divergence, which is not shown in the EMEX profile.[4] The lack of upper-level divergence in the EMEX data may have been a result of more attenuation at the shorter radar wavelength used by the aircraft radar in EMEX (3 cm) compared to the ground-based radars used in DUNDEE (5 cm), or may be an artifact of receiver thresholding in the radar system.

The wind profiler divergence composite (Fig. 8a) corresponds well with the single-Doppler results, especially when considering the large gradients observed in the individual profiles. Evidently, there is cancellation of much of the high-frequency variability in the profiler measurements so that only the dominant features are preserved in the composite. In the lower troposphere, the wind profiler composite shows a convergence peak centered at the melting layer and divergence below about 3 km, consistent with the single-Doppler results. The most significant difference between the wind profiler and single-Doppler composites is in the upper troposphere where the profiler measures a region of horizontal divergence above the single-Doppler composites.

The vertical motion composite profiles corresponding to horizontal divergence show qualitative agreement among the analysis methods in the lower troposphere, with a broad peak of descending motion centered near 3 km (Fig. 8b). The crossover location from low-level descent to upper-level ascent ranges from about 4.5 km in the CEVAD to about 10.5 km in the EVAD, on average. As expected from comparison of the distributions in Figs. 6 and 7, the CEVAD composite, although producing a similar divergence pattern to EVAD, shows deeper and larger ascent in the upper troposphere. The noisy appearance in the CEVAD profile is due to a combination of the low number of samples composited above about 11.5 km and the lack of constraint on the vertical motion at the top of the column. The noisiness may also have been mitigated if the radars had always scanned to higher elevation angles.

The wind profiler vertical motion composite shows qualitatively good agreement compared to the single-Doppler profiles with peak downward motion occur-

[4] The existence of of upper-level divergence in the EMEX composite was postulated by Mapes and Houze (1993) based on mass balance constraints.

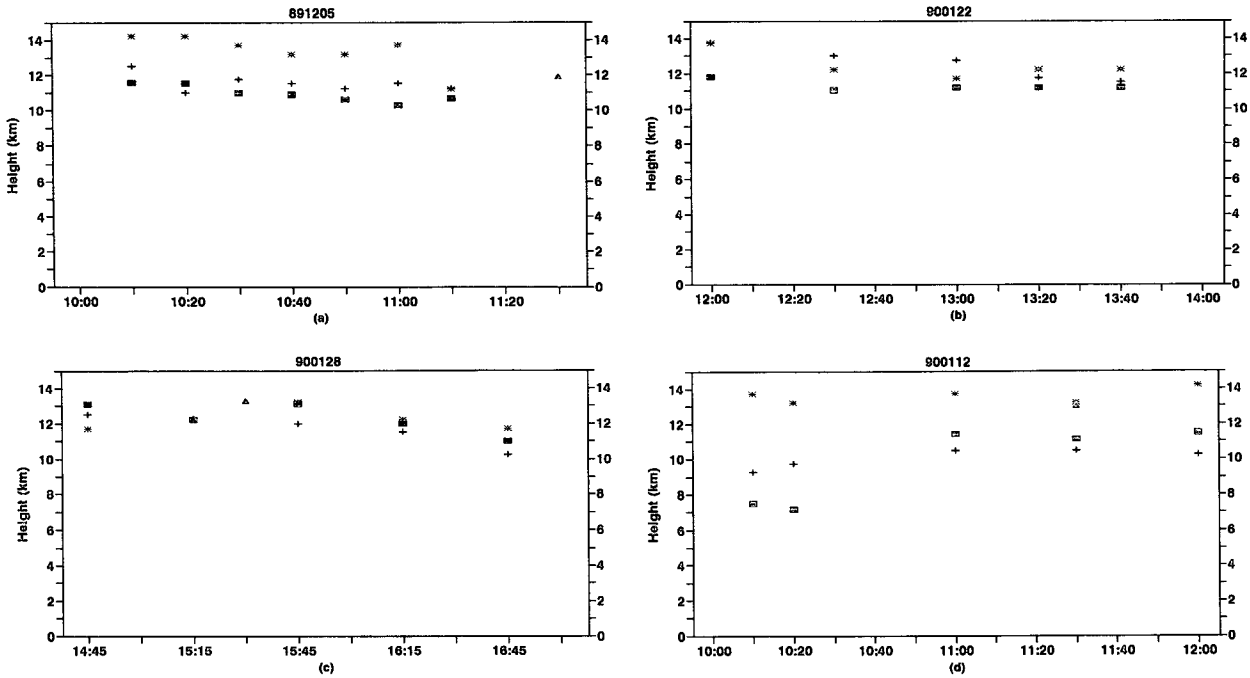

FIG. 10. Time–height cross sections showing the vertical velocity upper boundary for the (a) 5 December 1989 break regime MCS, (b) 22 January 1990 break regime MCS, (c) 28 January 1990 break regime MCS, and (d) 12 January 1990 monsoon regime MCS using the wind profiler (asterisk), VVP (plus sign), and EVAD–CEVAD (filled square) analysis methods. The absicca in each plot is time (UTC). Single-Doppler data points in (a), (b), and (d) are for the MIT radar while (c) is for the TOGA radar. Also included in (a), (c), and (d) are cloud-top height estimates based on GMS satellite imagery (filled triangle).

ring near 3 km and peak ascent near 10.5 km (Fig. 8b). The similarity is not necessarily to be expected, given the fact that the profiler vertical motion estimates at each height are independent. In contrast, the integration procedure forces the single-Doppler diagnosed vertical motion value at every height to contain some divergence information from elsewhere in the profile. Similar to the divergence composite, much of the high-frequency variability observed in the individual profiles of vertical motion has been smoothed in the average. In the upper troposphere, the wind profiler composite extends approximately 1.5 km above the single-Doppler profiles, consistent with the divergence profiles in Fig. 8a.

The standard deviation of the composite vertical velocity profiles are shown in Fig. 9. For each of the analysis methods, the variability of the profiles is comparable in magnitude to the composite mean, indicating a large degree of variability in the stratiform kinematic structure of the four MCSs or nonrobust models in the analysis methods. The single-Doppler profiles are all similar below about 6.5 km. However, the CEVAD composite standard deviation increases in magnitude at upper levels and appears more variable than the EVAD or VVP profiles. Again, the variability reflects the fact that the CEVAD vertical air velocity is not forced to zero at the upper boundary. The variability of the wind profiler composite is relatively constant throughout the profile, being larger than EVAD, CEVAD, or VVP in the lower troposphere and of similar magnitude to CEVAD in the upper troposphere.

c. *Radar and wind profiler sensitivity comparison*

In this section, we examine differences in the height of the radar and the wind profiler vertical motion upper boundary location for all of the analyses performed on the four MCSs. It is important to point out the practical use of an upper boundary condition. As discussed in section 2, all of the scanning radar methods require a top boundary in order to integrate the retrieved horizontal divergence and thereby diagnose vertical motion. The top boundary condition is only used as a proxy for setting $w = 0$, and an imperfect one at that, in EVAD and VVP. This is one of the weak features of these methods. The top of the column in CEVAD can be anywhere where w is not yet known, since w at the top boundary is solved for in the variational procedure.

Note that the upper boundary location in the scanning radar analyses does not necessarily coincide with cloud top (as inferred from GMS satellite imagery) or the maximum radar echo top height. Rather, the upper boundary represents the height, above which, insufficient data exists to perform a particular single-Doppler retrieval. The upper boundary is usually located some

distance below the cloud top or maximum radar echo height.

Time–height plots of the top of the single-Doppler analysis domain and the wind profiler upper boundary location for each MCS are shown in Fig. 10. The top boundary altitude of the single-Doppler domains differs greatly from the wind profiler upper boundary location for many of the simultaneous analyses. These differences are especially pronounced in the 5 December 1989 and 12 January 1990 MCSs where the wind profiler sampled vertical motion well above the single-Doppler radar. For all the available analysis times from all four MCSs, the wind profiler measured vertical motion an average of 1.9 km above the top of the EVAD–CEVAD upper boundary and 1.5 km above the VVP upper boundary. This result implies that the single-Doppler methods were underestimating the depth of divergence (vertical motion) occurring in the upper portion of the stratiform cloud.

It is important to note that the upper boundary of the wind profiler and scanning radar platforms is determined from different backscattering mechanisms: the scanning radar is dependent on Rayleigh scattering from a relatively even distribution of precipitation targets surrounding the radar while the wind profiler upper boundary is determined from thresholded Bragg scattering returns (i.e., gradients in the index of refraction; Gage 1990). The reflectivity associated with Bragg scatter has a weak dependence on wavelength compared to Rayleigh scattering from precipitation targets as shown below in (5):

$$\eta_a = 0.38 C_n^2 \lambda^{-1/3} \tag{5a}$$

$$\eta_p = \frac{\pi^5 |K|^2 Z_e}{\lambda^4}. \tag{5b}$$

In (5), η_a is the reflectivity associated with clear air, η_p is the reflectivity associated with precipitation, λ is wavelength, C_n^2 is the refractive index structure parameter, $|K|^2$ is the dielectric constant for water, and Z_e is the effective radar reflectivity factor. Equation (5) shows that the 5-cm scanning radar reflectivity is dominated by Rayleigh scattering from precipitation targets whereas the VHF wind profiler, operating at 6-m wavelength, is sensitive to backscatter from both precipitation and turbulence echoes (e.g., Ralph 1995).

Given the strict precipitation echo requirements imposed by the single-Doppler techniques, it is not surprising that the top level in these methods was often below the corresponding wind profiler upper boundary. Lemone and Jorgensen (1991) also observed similar situations where the diagnosed vertical motion field was underestimated because of inadequate measurements of upper-level divergence (and assuming $w = 0$ at the radar echo top). Moreover, Mapes and Houze (1995) presented a radial velocity vertical cross section from a tropical MCS where the peak upper-level divergence occurred at the height of the scanning radar precipitation echo top. The implication in the Mapes and Houze study is that a significant amount of air was diverging above the radar precipitation echo-top boundary (i.e., diverging into the clear air) which could not be detected by the scanning radars. Taken together, the results from this and previous studies suggest that the ability of scanning radars to adequately measure upper-level divergence can be limited in some situations.

5. Conclusions

We have examined the structure of vertical velocity and horizontal divergence in the stratiform region of several tropical MCSs based on simultaneous collection of vertically pointing wind profiler and single-Doppler radar data. The location of the scanning radars with respect to the wind profiler provided for considerable overlap in the sampling region and allowed for a comparison of the precipitating region kinematic structure at both the mesoscale and submesoscale.

In regard to the scanning radar data, the results of several retrieval techniques (EVAD, CEVAD, VVP) were compared on multiple volumes of radar data. All of these techniques make assumptions about variations in the horizontal wind across the analysis domain in order to transform the measured radial wind field into a two-dimensional horizontal wind vector, calculate horizontal divergence through a least squares solution of the model, and then use the mass continuity equation to calculate a profile of vertical velocity. In the vertical velocity calculation, both EVAD and VVP make assumptions about the magnitude of vertical air motion at the top of the column, whereas CEVAD imposes a constraint on particle terminal fall speed.

All of the single-Doppler techniques documented the existence of low-level divergence and mostly midtropospheric convergence. The greatest variability in the retrieved profiles occurred at upper levels where the VVP profile often extended to greater height that the corresponding EVAD or CEVAD profiles. The difference in the top boundary location is due to the more stringent echo coverage requirement imposed by EVAD–CEVAD as opposed to VVP. The difference between the EVAD and VVP vertical motion profiles were large for one particular case due to the occurrence of nonuniform echo coverage in the upper portion of the stratiform cloud. In this case, the EVAD method could not analyze data high enough in the cloud to diagnose divergence and subsequently produced deep downward motion in the profile, since the vertical velocity was set to zero at the top of the analysis domain. The performance of both EVAD and VVP could probably have been improved by using more customized scans.

The CEVAD method produced vertical motion profiles that commonly showed deeper and larger magnitude ascending motion than EVAD, despite nearly

identical profiles of divergence. This difference occurred because of the CEVAD constraint on particle terminal fall speed at the top boundary (as opposed to vertical air motion) and because of the requirement that all the vertical layers in the analysis volume adjust concurrently during the regression solution. Apparently, this methodology renders the CEVAD solution less susceptible to underestimating upper-level divergence compared to EVAD. These results emphasize the potential uncertainties involved in diagnosing vertical motion from a retrieved profile of divergence.

The wind profiler, because of its vertically pointing beam configuration, sampled a much smaller volume compared to the scanning Doppler radars. Consistent with the sampling geometry, the vertical motion and divergence fields generated with the wind profiler were more variable and of larger magnitude than the corresponding single-Doppler generated profiles, suggesting that small-scale (submesoscale) vertical circulations occurred in the stratiform region of these MCSs that were revealed with the wind profiler but not the single-Doppler retrievals. In this sense, the wind profiler compliments the scanning radar as an observing tool since it can reveal small-scale kinematic features in precipitating regions and continues to measure in echo-free conditions. However, detailed comparisons of the vertical motion differences between the single-Doppler and wind profiler at any given height are limited by the real small-scale variability (and sometimes larger noise) in the wind profiler estimates.

It is not known the extent to which submesoscale vertical motion fluctuations in the stratiform portion of an MCS would effect the large-scale in terms of heat, moisture, and momentum budgets. It is possible, however, that the existence of small-scale circulations in the stratiform region could have a significant impact on precipitation growth mechanisms and the resulting rainfall flux, which deserves further study.

When all of the available data for each method were composited, there was relatively good qualitative agreement between the wind profiler and single-Doppler profiles in the lower and middle troposphere. Much of the high-frequency variability observed in the individual wind profiler retrievals was reduced so that only the dominant features were preserved in the composite. The composites from all the methods showed a convergence peak near the melting level with a corresponding region of peak descent near 3 km. However, the wind profiler data showed that significant divergence (upward motion) frequently occurred above the top of the VVP and EVAD–CEVAD single-Doppler analysis domains. On average, the profiler diagnosed vertical motion about 2 km above the EVAD–CEVAD analysis domain and 1.5 km above the VVP analysis domain. These results suggest that the radars were underestimating the upper-level divergence regardless of the analysis method used.

Acknowledgments. This work was supported by the Contract NA37RJ0202 from NOAA (Office of Global Programs-TOGA/COARE). Drs. Ken Gage, Warner Ecklund (both of the NOAA/Aeronomy Lab), Michael Manton, and Tom Keenan (from BMRC) played key roles in establishing the Darwin profiler site. Doug Burks and Dr. Takmeng Wong (both formerly of CSU) assisted in the data analysis and data collection, respectively. Dr. Anthony Riddle of the NOAA Aeronomy lab assisted in the interpretation of wind profiler spectra data. Drs. P. May of BMRC, Martin Ralph of NOAA ETL, and Walt Petersen of CSU also contributed to this research. The two anonymous reviewers are acknowledged for their constructive comments.

REFERENCES

Augustine, J. A., and E. J. Zipser, 1987: The use of wind profilers in a mesoscale experiment. *Bull. Amer. Meteor. Soc.*, **68,** 4–17.

Balsley, B. B., W. L. Ecklund, D. A. Carter, A. C. Riddle, and K. S. Gage, 1988: Average vertical motions in the tropical atmosphere observed by a radar wind profiler on Pohnpei (7°N latitude, 157°E longitude). *J. Atmos. Sci.*, **45,** 396–405.

Biggerstaff, M. I., and R. A. Houze Jr., 1993: Kinematics and microphysics of the transition zone of the 10–11 June 1985 squall line. *J. Atmos. Sci.*, **50,** 3091–3110.

Boccippio, D. J., 1995: A diagnostic analysis of the VVP single-Doppler retrieval technique. *J. Atmos. Oceanic Technol.*, **12,** 230–248.

Brandes, E. A., and C. L. Ziegler, 1993: Mesoscale downdraft influences on vertical vorticity in a mature mesoscale convective system. *Mon. Wea. Rev.*, **121,** 1337–1353.

Browning, K. A., and R. Wexler, 1968: The determination of kinematic properties of a wind field using Doppler radar. *J. Appl. Meteor.*, **7,** 105–113.

Carter, D. A., W. L. Ecklund, J. R. McAfee, K. S. Gage, T. Keenan, and M. Manton, 1991: Results from the first year of observations using the Darwin VHF wind profiler. Preprints, *25th Int. Conf. on Radar Meteorology,* Paris, France, Amer. Meteor. Soc., 288–291.

Chilson, P. B., C. W. Ulbrich, M. F. Larsen, P. Perillat, and J. E. Keener, 1993: Observations of a tropical thunderstorm using a vertically pointing, dual-frequency, collinear beam Doppler radar. *J. Atmos. Oceanic Technol.*, **10,** 663–673.

Cifelli, R., and S. A. Rutledge, 1994: Vertical motion structure in Maritime Continent mesoscale convective systems: Results from a 50-MHz profiler. *J. Atmos. Sci.*, **51,** 2631–2652.

——, W. Petersen, and D. J. Boccippio, 1994: Ship-based single and dual-Doppler analyses of TOGA COARE convective systems. Preprints, *Sixth Conf. on Climate Variations,* Nashville, TN, Amer. Meteor. Soc., J58–J62.

Gage, K. S., 1990: Radar observations of the free atmosphere: Structure and dynamics. *Radar in Meteorology,* D. Atlas, Ed., Amer. Meteor. Soc., 534–565.

Gamache, J. F., and R. A. Houze Jr., 1982: Mesoscale air motions associated with a tropical squall line. *Mon. Wea. Rev.*, **110,** 118–135.

Heymsfield, G. M., and S. Schotz, 1985: Structure and evolution of a severe squall line over Oklahoma. *Mon. Wea. Rev.*, **113,** 1563–1589.

Houze, R. A., Jr., 1982: Cloud clusters and large-scale vertical motions in the tropics. *J. Meteor. Soc. Japan,* **60,** 396–409.

——, 1989: Observed structure of mesoscale convective systems and implications for large-scale heating. *Quart. J. Roy. Meteor. Soc.*, **115,** 425–461.

Johnson, R. H., and D. C. Kriete, 1982: Thermodynamic and circulation characteristics of winter monsoon tropical mesoscale convection. *Mon. Wea. Rev.*, **110,** 1898–1911.

——, and G. S. Young, 1983: Heat and moisture budgets of tropical mesoscale anvil clouds. *J. Atmos. Sci.*, **40,** 2138–2147.

Keenan, T. D., and S. A. Rutledge, 1993: Mesoscale characteristics of monsoonal convection and associated stratiform precipitation. *Mon. Wea. Rev.*, **121,** 352–374.

Koscielny, A. J., R. J. Doviak, and R. Rabin, 1982: Statistical considerations in the estimation of divergence from single-Doppler radar and application to prestorm boundary-layer observations. *J. Appl. Meteor.*, **21,** 197–210.

Larsen, M. F., S. Fukao, O. Aruga, M. D. Yamanaka, T. Tsuda, and S. Kato, 1991: A comparison of VHF radar vertical-velocity measurements by a direct vertical-beam method and by a VAD technique. *J. Atmos. Oceanic Technol.*, **8,** 766–776.

LeMone, M. A., and D. P. Jorgensen, 1991: Precipitation and kinematic structure of an oceanic mesoscale convective system. Part II: Momentum transport and generation. *Mon. Wea. Rev.*, **119,** 2638–2653.

Mapes, B., and R. A. Houze Jr., 1993: An integrated view of the 1987 Australian monsoon and its mesoscale convective systems. II: Vertical structure. *Quart. J. Roy. Meteor. Soc.*, **119,** 733–754.

——, and ——, 1995: Diabatic divergence profiles in western Pacific mesoscale convective systems. *J. Atmos. Sci.*, **52,** 1807–1828.

Matejka, T., 1993: Concurrent Extended Vertical Velocity Azimuth Display (CEVAD) analysis of single-Doppler radar data. Preprints, *26th Int. Conf. on Radar Meteorology,* Norman, OK, Amer. Meteor. Soc., 463–465.

——, and R. C. Srivastava, 1991: An improved version of the extended velocity–azimuth display analysis of single-Doppler radar data. *J. Atmos. Oceanic Technol.*, **8,** 453–466.

O'Brien, J. J., 1970: Alternative solutions to the classical vertical velocity problem. *J. Appl. Meteor.*, **9,** 197–203.

Ralph, F. M., 1995: Using radar-measured radial vertical velocities to distinguish precipitation scattering from clear-air scattering. *J. Atmos. Oceanic Technol.*, **12,** 257–267.

——, M. Crochet, and S. V. Venkateswaran, 1993: Observations of a mesoscale ducted gravity wave. *J. Atmos. Sci.*, **50,** 3277–3291.

Ramage, C. S., 1968: Role of a tropical "Maritime Continent" in the atmospheric circulation. *Mon. Wea. Rev.*, **96,** 365–370.

Rutledge, S. A., 1991: Middle latitude and tropical mesoscale convective systems. *Rev. Geophys.* (Suppl.), **29,** 88–97.

——, E. R. Williams, and T. D. Keenan, 1992: The Down Under Doppler and Electricity Experiment (DUNDEE): Overview and preliminary results. *Bull. Amer. Meteor. Soc.*, **73,** 3–16.

——, R. A. Houze Jr., M. I. Biggerstaff, and T. Matejka, 1988: The Oklahoma–Kansas mesoscale convective system of 10–11 June 1985: Precipitation structure and single-Doppler radar analysis. *Mon. Wea. Rev.*, **116,** 1409–1430.

Sato, T., H. Doji, H. Iwai, I. Kimura, S. Fukao, M. Yamamoto, T. Tsuda, and S. Kato, 1990: Computer processing for deriving drop-size distributions and vertical air velocities from VHF Doppler radar spectra. *Radio Sci.*, **25,** 961–973.

Srivastava, R. C., T. J. Matejka, and T. J. Lorello, 1986: Doppler radar study of the trailing anvil region associated with a squall line. *J. Atmos. Sci.*, **43,** 356–377.

Wakasugi, K., A. Mizutani, M. Matsuo, S. Fukao, and S. Kato, 1986: A direct method for deriving drop-size distribution and vertical air velocities from VHF Doppler radar spectra. *J. Atmos. Oceanic Technol.*, **3,** 623–629.

——, ——, ——, ——, and ——, 1987: Further discussion on deriving drop-size distribution and vertical air velocities from VHF Doppler radar spectra. *J. Atmos. Oceanic Technol.*, **4,** 170–179.

Waldteufel, P., and H. Corbin, 1979: On the analysis of single-Doppler radar data. *J. Appl. Meteor.*, **18,** 532–542.

Yoe, J. G., M. F. Larsen, and E. J. Zipser, 1992: VHF wind-profiler data quality and comparison of methods for deducing horizontal and vertical air motions in a mesoscale convective storm. *J. Atmos. Oceanic Technol.*, **9,** 713–727.

Yuter, S. E., and R. A. Houze Jr., 1995: Three-dimensional kinematic and microphysical evolution of Florida cumulonimbus. Part II: Frequency distributions of vertical velocity, reflectivity, and differential reflectivity. *Mon. Wea. Rev.*, **123,** 1941–1963.

Zipser, E. J., 1969: The role of organized unsaturated convective downdrafts in the structure and rapid decay of an equatorial disturbance. *J. Appl. Meteor.*, **8,** 799–814.